RSC Advances

ROYAL SOCIETY OF CHEMISTRY

www.rsc.org/advances

Preparation and characterization of composite magnetic photocatalyst $Mn_xZn_{1-x}Fe_2O_4/\beta\text{-}Bi_2O_3$

Zhaodi Zhang[a], Longjun Xu[a*], Chenglun Liu[b]

[a] *State Key Laboratory of Coal Mine Disaster Dynamics and Control, Chongqing University, Chongqing 400044, PR China*

[b] *College of Chemistry and Chemical Engineering, Chongqing University, Chongqing 400044, PR China*

*Corresponding author: E-mail: xulj@cqu.edu.cn

Abstract: Composite magnetic photocatalyst $Mn_xZn_{1-x}Fe_2O_4/\beta\text{-}Bi_2O_3$ was synthesized by dip-calcination method using manganese zinc ferrite as magnetic substrate. The effects of composite mass ratio, reaction time and calcination temperature on the degradation of Rhodamine B(RhB) under the simulated sunlight were discussed by tests. The as-prepared $Mn_xZn_{1-x}Fe_2O_4/\beta\text{-}Bi_2O_3$ was characterized by XRD, FTIR, VSM, UV-vis DRS and SEM. The photodegradation rate of RhB in $Mn_xZn_{1-x}Fe_2O_4/\beta\text{-}Bi_2O_3$ was higher (99.1%) than that (83.6%) of pure $\beta\text{-}Bi_2O_3$ within 2.5h. XRD spectra revealed that the composites presented tetragonal type, which was similar to that of $\beta\text{-}Bi_2O_3$. There were peaks both of Bi-O bonds and $Mn_xZn_{1-x}Fe_2O_4$ absorption in FTIR spectra. The saturation magnetization (Ms) and coercivity (Hc) of composite photocatalyst were 7.01A·m^2/kg and 25.38 A/m, respectively. DRS analysis revealed that the optical band gap of this composite was 2.31eV, which was lower than that (2.45eV) of $\beta\text{-}Bi_2O_3$. Moreover, the photocatalytic activity still maintained 82.7% after five cycles. The magnetic property with an appropriate amount of manganese zinc ferrite inhibited the recombination of photo-produced electrons (e^-) and holes (h^+), and enhanced the photocatalytic property of $\beta\text{-}Bi_2O_3$.

Keywords: Magnetic photocatalyst; $Mn_xZn_{1-x}Fe_2O_4/\beta\text{-}Bi_2O_3$; Photocatalytic activity; Recycling;

1. Introduction

TiO_2 had been widely utilized as a promising catalyst for photochemistry oxidation since Fujishima and Honda et al firstly applied the catalyst for electrochemical proteolysis of water in 1972 [1]. Cary et al (1972) thought that TiO_2 showed promise as semiconductor photocatalyst for the degradation of organics in water [2]. It meant that TiO_2 was adapted to be employed in the field of environmental pollutants control. Frank et al (1977) found further applications of photocatalytic oxidation technology for degrading pollutants from industrial waste water [3-5]. These contributions had laid the theoretical foundation and proven the considerable serviceability of TiO_2 as a promising photocatalyst for pollutants control [6-8].

Due to wide band gap and weak response to visible light of TiO_2, intensive attentions have recently been directed towards exploring novel photocatalysts such as Ag_3PO_4 and their composites [9, 10], sulfides [11], bismuth compounds [12-14], and doping metals or nonmetals [15]. Bismuth compounds of Bi_2O_3 have recently been considered as a preferable option for the synthesis of optical catalyst, due to its narrower band gap and larger absorption wavelength. Bi_2O_3 has four polymorphs, namely α，β，γ，δ. Their band gaps are 2.85, 2.58, 2.68 and 2.75 eV, respectively [16-18]. $\beta\text{-}Bi_2O_3$ is superior to the $\alpha\text{-}Bi_2O_3$ in photocatalytic properties. However, most traditional and new photocatalyst in the photocatalytic reaction system present in suspension state, which makes separation rather difficult of the materials, let alone recycle and reuse. The problem seriously restricts the effective

utilization of photocatalysts and causes more consume energy and cost-intensive in the photocatalytic process. It is noteworthy to develop a composite magnetic photocatalyst to be recycled by an external magnetic field [19-20]. The magnetic photocatalyst is expected to overcome the difficulty of recycling photocatalyst in suspension state.

$Mn_xZn_{1-x}Fe_2O_4$, which is a typical magnetic material, owns several advantages of high saturation magnetization and permeability, large production efficiency, stable performance and excellent corrosion resistance [21-22], comparing with traditional metallic soft magnetic materials (e.g. Fe_3O_4). There were few researches about $Mn_xZn_{1-x}Fe_2O_4$ involved in composite magnetic photocatalyst up today. Wang et al prepared magnetic photocatalyst of $TiO_2/Mn_xZn_{1-x}Fe_2O_4$/AC with Sol-gel method, and they reported that the as-synthesized catalyst presented superior photocatalytic activity over pure TiO_2 under ultraviolet light [23]. In our previous work, we have prepared magnetic solid acid catalyst $S_2O_8^{2-}/ZrO_2$-$Mn_xZn_{1-x}Fe_2O_4$ based on magnetic matrix $Mn_xZn_{1-x}Fe_2O_4$[19]. It was found that the as-prepared magnetic solid acid catalyst has higher catalytic activity on the transesterification respect than pure substance. In the present work, $Mn_xZn_{1-x}Fe_2O_4$ was chosen as magnetic substrate, and composite magnetic photocatalyst $Mn_xZn_{1-x}Fe_2O_4/\beta$-$Bi_2O_3$ was synthesized by dip-calcination method. The photocatalytic activity of the as-prepared catalyst was then tested under simulated sunlight. Further insights have been focused on the mechanism and recycling feasibility with external magnetic field. The results in this work will lay the groundwork for further application of the photocatalyst in pollutants removal.

2. Experimental

Analytical reagents of $Bi(NO_3)_3$, Na_2CO_3, $FeCl_3$, $ZnSO_4$ and HNO_3 were used as raw materials for sample preparation, and provided by Shanghai Jiuyi Chemical Ltd. $MnSO_4$ solution was leached and refined from manganese ore[24].

2.1 Preparation of β-Bi_2O_3

3.12g $Bi(NO_3)_3 \cdot 5H_2O$ was dissolved in 20mL diluted HNO_3 solution , stirring for 2 hours. The $Bi(NO_3)_3$-HNO_3 solution was slowly added into 0.6 mol/L Na_2CO_3 solution and stirred for 2 hours at ambient temperature [25]. The obtained precipitates were filtered and washed in deionized water for several times, and the precipitates were dried at 60℃. After that, the dry blocks were crushed into fine powder and calcined at 380℃ in pure N_2 atmosphere for 10 minutes, and then the bright yellow of β-Bi_2O_3 was obtained.

2.2 Preparation of $Mn_xZn_{1-x}Fe_2O_4/\beta$-$Bi_2O_3$

In the molar ratio of n (ZnO): n (MnO): n (Fe_2O_3)=13.3:32.8:53.9, the defined dosage of $ZnSO_4$, $MnSO_4$ and $FeCl_3 \cdot 6H_2O$ was respectively dissolved in deionized water, and the solution was stirred with a mechanical stirrer for 30minutes at ambient temperature. Subsequently, the as-prepared $ZnSO_4$ solution and $FeCl_3$ solution were added to $MnSO_4$ solution under the condition of continuous stirring, then the mixture solution was gained. The definite amount of $(NH_4)_2C_2O_4 \cdot H_2O$ was dissolved in deionized water, and formed $(NH_4)_2C_2O_4$ solution. The mixture solution was slowly added to $(NH_4)_2C_2O_4$ solution after the mixture solution and $(NH_4)_2C_2O_4$ solution were heated to 80℃, respectively. The pH value of the system was adjusted to 7, and a great amount of precipitate presented. The mixtures were filtrated; the precipitate was washed with the deionized water and dried at 80℃ for 12 hours. The residues were sintered at 1200℃ for 3 hours, magnetic $Mn_xZn_{1-x}Fe_2O_4$ was obtained.

$Mn_xZn_{1-x}Fe_2O_4$ with the mass ratio of 15 wt% was added into the above $Bi(NO_3)_3$-HNO_3 solution and stirred for 30 minutes. The mixture was then added dropwise to 0.6mol/L Na_2CO_3 solution, and stirred mechanically for 2 hours at ambient temperature. After filtration, the residue was washed for

several times with deionized water and the precipitate was dried at 60℃. The composite $Mn_xZn_{1-x}Fe_2O_4/\beta$-$Bi_2O_3$ (15 wt%) was produced by sintering the dried filter residue at 380℃ for 10 minutes. A series of composites $Mn_xZn_{1-x}Fe_2O_4/\beta$-$Bi_2O_3$ with was synthesized by adjusting the mass ratios of $Mn_xZn_{1-x}Fe_2O_4$ and β-Bi_2O_3(5 wt %, 10 wt%, 15 wt%, 20 wt%, 25 wt%). In addition, the composites $Mn_xZn_{1-x}Fe_2O_4/\beta$-$Bi_2O_3$ were prepared at the various reaction time (1h, 1.5h, 2h, 2.5h, 3h) and the calcination temperature (360℃, 370℃, 380℃, 390℃, 400℃).

2.3 Characterization of $Mn_xZn_{1-x}Fe_2O_4/\beta$-$Bi_2O_3$

Phase identification of as-prepared products was performed with X-ray diffractometer (Shimadzu XRD-6000) at a scanning rate of $4°\cdot min^{-1}$ with the 2θ range of 10°-80°. Fourier transform infrared spectroscopy (FTIR) spectra of samples were recorded on a 5DX FTIR spectrometer (5DX, Nicolet. Co., USA). The products' morphologies and microstructures were observed by scanning electron microscopy (SEM, Hitachi S-4800, Japan). The UV-vis diffuse reflectance spectra (DRS) and the magnetic properties of tested-samples were respectively measured using a UV-vis spectrophotometer (TU1901, China) and a vibrating sample magnetometer (MPMS-XL-7 Quantum Design, USA). Element contents in the composite were analyzed by ICP (Inductively Coupled Plasma Spectrometer, ICP 6300 series, Thermo scientic Co.,USA). The concentration of the composite solution was 500μg/mL to meet the detection range of ICP spectrometer.

2.4 Measurement of photocatalytic property

The photocatalytic activity of $Mn_xZn_{1-x}Fe_2O_4/\beta$-$Bi_2O_3$ was evaluated by the degradation of Rhodamine B (RhB) under simulated sunlight. 100mL of RhB aqueous solution (10 mg/L) and 0.2g photocatalyst were added into quartz container and stirred for 1 hour in the dark to reach adsorption and desorption balance. Then, the Xenon lamp(CEL-HXF3000, AULTT) of 300W was employed light resource and the solution was irradiated for 2.5 hours in the process of continuous stirring. 5mL RhB solution was withdrawn in setting time interval. Then the mixtures were centrifuged at 3800 rpm for 10 minutes to obtain the supernatant. The photocatalytic degradation process of RhB was monitored by measuring its characteristic absorption at 554 nm with an UV-vis spectrophotometer.

3. Results and discussion

3.1 Optimization condition of $Mn_xZn_{1-x}Fe_2O_4/\beta$-$Bi_2O_3$ preparation

The effects of mass ratio, reaction time and calcination temperature on the degradation rate of RhB were investigated by tests. It was discovered from Table 1 that the degradation rate increased at first and then decreased with the increases of $Mn_xZn_{1-x}Fe_2O_4/\beta$-$Bi_2O_3$ mass ratio from 5 wt% to 25 wt%. The maximum degradation rate reached when the mass ratio was 15 wt%. The reason was that photo-produced electrons (e^-) and holes (h^+) was not easy to separate effectively when the loading amount of $Mn_xZn_{1-x}Fe_2O_4$ was low. The magnetic field generated by an appropriate amount of $Mn_xZn_{1-x}Fe_2O_4$ reduced the recombination of photo-produced electrons (e^-) and holes (h^+), and extended the lifetime of photo-produced electrons. Thereby, the photocatalytic activity of the composite was improved. However, the photocatalytic activity did not appear the enhancement with the ever-increasing loading amounts of $Mn_xZn_{1-x}Fe_2O_4$. Since $Mn_xZn_{1-x}Fe_2O_4$ itself was a semiconductor, too much $Mn_xZn_{1-x}Fe_2O_4$ loaded in β-Bi_2O_3 resulted in a great large number of recombination center of photo-produced electrons (e^-) and holes (h^+). The photocatalytic active property of this catalyst declined.

It was discovered from Table 1 that the photocatalytic activity of 15 wt% $Mn_xZn_{1-x}Fe_2O_4/\beta$-$Bi_2O_3$ increased first and decreased later with the increase of time within 3 hours. The largest photocatalytic activity of β-Bi_2O_3 reached at the reaction time of 2 hours. The effect of calcination temperature on the

photocatalytic activity of $Mn_xZn_{1-x}Fe_2O_4/\beta$-$Bi_2O_3$(15 wt%) was investigated in the optimal time of 2 hours. It was found that the photocatalytic activity increased with the increase of calcination temperature from 360℃ to 380℃, and then the activity dropped with the further increase of calcination temperature. The excellent photocatalytic activity achieved at 380℃ of calcination temperature. The result was mostly caused by α-Bi_2O_3 at higher calcination temperature, as the photocatalytic activity of α-Bi_2O_3 was much lower than that of β-Bi_2O_3. At the same time, the low activity of β-Bi_2O_3 at lower calcination temperature was related to the incomplete conversion of crystalline.

The orthogonal experiments with three factors and three levels were carried out to obtain the optimal synthesis condition of the photocatalyst. The results were shown in Table 2 and proved again that the large photocatalytic activity presented under the condition of the mass ratio of 15%, the reaction time of 2 hours and the calcination temperature of 380℃. The experiments demonstrated in further that calcination temperature was the key factor to impact the photocatalytic activity. The importance order of impact factors in the photocatalytic activity were calcination temperature>mass ratio>reaction time. The conclusion in the orthogonal experiments was consistent with the result of the single-factor experiment.

3.2 Structure characteristics

X-ray diffraction peaks of β-Bi_2O_3 and $Mn_xZn_{1-x}Fe_2O_4$ as well as $Mn_xZn_{1-x}Fe_2O_4/\beta$-$Bi_2O_3$(15 wt%) were sharp and symmetrical in Fig.1. It was deduced that there were good crystallinity in as-prepared products. It was worth to notice that the characteristic spectra of β-Bi_2O_3 were evidently indexed with the standard card (JCPDS card number: 27-0050), corresponding to diffraction phases of (201), (220), (222) and (421) exactly. It was reasonable to ensure that the as-prepared β-Bi_2O_3 belonged to tetragonal type. The diffraction peaks of $Mn_xZn_{1-x}Fe_2O_4/\beta$-$Bi_2O_3$(15 wt%) were consisted with each diffraction phase of β-Bi_2O_3 in Fig.1(c). It was natural to conclude the crystallinity integral of β-Bi_2O_3.

It meant that $Mn_xZn_{1-x}Fe_2O_4$ did not change the structure of β-Bi_2O_3 itself. There were not any diffraction peaks of $Mn_xZn_{1-x}Fe_2O_4$ in XRD pattern of $Mn_xZn_{1-x}Fe_2O_4/\beta$-$Bi_2O_3$(15 wt%). It was explained that $Mn_xZn_{1-x}Fe_2O_4$ was too little to be detected by X-Ray diffraction. In addition, the peaks of $Mn_xZn_{1-x}Fe_2O_4$ were covered by strong diffraction peaks of β-Bi_2O_3. The existence of $Mn_xZn_{1-x}Fe_2O_4$ was confirmed by measurements of ICP, FTIR and SEM.

The qualitative analysis of the as-prepared product was performed with ICP, and its principle is that each element creates its own unique spectrum when it is activated. Therefore, an element can be confirmed according to the existence of its corresponding spectral line. Three groups of data were listed in the Table 3. There was the element of Bi in $Mn_xZn_{1-x}Fe_2O_4/\beta$-$Bi_2O_3$ (15 wt%) as the signal average of Bi was 8:1:16. In the same way, the existence of other elements including Mn and Zn as well as Fe in the tested sample was proved by this detection. It indicated that there were the elements of Mn , Zn, Fe and Bi in the composite catalyst. The wavelengths corresponding to the minimum detectability for Mn , Zn , Fe and Bi were respectively 257.6nm, 213.8nm, 259.9nm and 223.0nm, and consistent with the data reported in the literature[26-28].

FTIR spectra of $Mn_xZn_{1-x}Fe_2O_4$, β-Bi_2O_3, $Mn_xZn_{1-x}Fe_2O_4/\beta$-$Bi_2O_3$(15 wt%) and recovery composites(1#, 2#, 3#, 4#) was shown in Fig.2. The characteristic spectra at 3448.3 cm^{-1} and 1637.0 cm^{-1} (green lines) was contributed the stretching vibration and deformation vibration of hydroxyl group (-OH) in adsorption water from wet atmosphere. Sample 1 showed that three characteristic peaks of $Mn_xZn_{1-x}Fe_2O_4$ were at 1118.1cm^{-1} and 556.6cm^{-1} as well as 436.6 cm^{-1} (blue lines) [24], respectively. The intensive signal around 1394.1 cm^{-1} and 846.4 cm^{-1} as well as 521.6 cm^{-1} (red lines) appeared in FTIR spectrum of β-Bi_2O_3 was referable to the stretching vibration of Bi-O bonds[29]. At the same

time, sample 4 was FTIR pattern of recovery composite washed with ethanol. It was noticed that there were characteristic peaks both of β-Bi_2O_3 and $Mn_xZn_{1-x}Fe_2O_4$ in the recovery tested sample, and no any impurity peaks appeared. The result illustrated that RhB dye molecules were not adsorbed in the composite particles after the photocatalytic degradation tests of RhB were end. This dye did remove from the solution with the photocatalyst under the light illumination. There were a little wave shift of the characteristic peaks in FTIR spectra of both β-Bi_2O_3 and $Mn_xZn_{1-x}Fe_2O_4$ for the vibration coupling between the peaks of $Mn_xZn_{1-x}Fe_2O_4$ and Bi_2O_3 bonds. It was important that the characteristic peaks were fairly obvious in this pattern.

Fig.3 showed SEM images of $Mn_xZn_{1-x}Fe_2O_4$ and β-Bi_2O_3 as well as $Mn_xZn_{1-x}Fe_2O_4$/β-Bi_2O_3(15 wt%). It was showed that $Mn_xZn_{1-x}Fe_2O_4$ was particles with irregular shape in Fig.3(a). As can be seen from Fig.3(b), β-Bi_2O_3 displayed nanoscale irregular granular of flake, rod-like and spherical. The irregular β-Bi_2O_3 particle and $Mn_xZn_{1-x}Fe_2O_4$ were complexed together successfully as showed in Fig.3(c-d). In details, β-Bi_2O_3 granular in the composite was smaller than that in pure Bi_2O_3, but the favor growth direction did not alter in the composite system. The surface flat did not get significant defects in the loading process of $Mn_xZn_{1-x}Fe_2O_4$. As we all know, the defect of surface on photocatalyst usually was a regeneration center for photo-produced electrons (e^-) and holes(h^+). Thus, the morphology structure of $Mn_xZn_{1-x}Fe_2O_4$/β-Bi_2O_3 was conducive to improve the photocatalytic activity.

3.3 Absorption light ability and magnetic property

The light absorption was an important property of semiconductors. The optical band gap energy (E_g) was directly related to the light absorbance. E_g was estimated with Equ.(1):

$$\alpha h\nu = C(h\nu - E_g)^{1/2} \quad (1)$$

Where, α was absorbance, h was Planck constant, and ν was photonic frequency, C was an experience constant.

Fig.4 showed diffuse reflectance spectra, corresponding band gap of pure β-Bi_2O_3 (a) and composite magnetic photocatalyst $Mn_xZn_{1-x}Fe_2O_4$/β-Bi_2O_3(15 wt %)(b). β-Bi_2O_3 was a kind of direct transition[25,30], the curve fitted by Equ.(1) was shown in Fig.4. It was clearly seen from Fig.4 that E_g of β-Bi_2O_3 and $Mn_xZn_{1-x}Fe_2O_4$/β-Bi_2O_3 (15 wt%) were 2.45ev and 2.31ev, respectively. The result was in accordance with literatures[31-32]. It was clear that both pure β-Bi_2O_3 and the composite held strong absorption in UV light region (wavelength: 200-400nm). However, it was worth noting that the composite showed a strong absorption in a wide wavelength range from UV to visible light, comparing to that of pure β-Bi_2O_3. What is specifically more, the maximum absorption wavelength of the composite increased to 537nm. Therefore, the visible light absorption ability of 15 wt% $Mn_xZn_{1-x}Fe_2O_4$/β-Bi_2O_3 was enhanced, the composite was adapted to employed visible catalyst.

The magnetic hysteresis loop of $Mn_xZn_{1-x}Fe_2O_4$ and the composite $Mn_xZn_{1-x}Fe_2O_4$/β-Bi_2O_3 (15 wt%) were displayed in Fig.5. It was gained in Fig.5 that the saturation magnetization(M_s) and remanent magnetization(M_r) of $Mn_xZn_{1-x}Fe_2O_4$/β-Bi_2O_3 (15 wt%) were 7.01 and 0.39 $A \cdot m^2 \cdot kg^{-1}$, respectively. Larger Ms was conducive to the separation and the recovery of the composite after the photocatalytic tests ended. Comparing to $Mn_xZn_{1-x}Fe_2O_4$, M_s and M_r of 15 wt% $Mn_xZn_{1-x}Fe_2O_4$/β-Bi_2O_3 declined by 91.6% and 88.4%, respectively. The declination was due to the decrease of the magnetic substance for per unit mass. Some β-Bi_2O_3 attached on the surface of $Mn_xZn_{1-x}Fe_2O_4$ also took an adverse role on the magnetic property.

3.4 Photocatalytic activity

The photocatalytic mechanism of semiconductor was stated as follows, the photocatalytic process

of β-Bi_2O_3 was conducted by enough stimulated energy photons. Valence band electronics of semiconductor excited energy grade transition for much photo-induced electron-hole pairs as β-Bi_2O_3 can absorb enough energy. Photo-electrons and holes migrated to the surface of the composite catalyst. That is to say, the dissolved oxygen was restored to the superoxide anions, at the same time, hydroxide ions and water were oxidized to the hydroxyl radicals (·OH) by electron-holes. With very strong oxidation resistance, superoxide anions and hydroxyl radicals (·OH) oxidized the most organics to the final products of CO_2 and H_2O[33-35], and broke down some inorganic completely to achieve the purpose of the degradation of pollutants.

The photocatalytic degradation rate of RhB with pure β-Bi_2O_3 reached to 83.6% at 2.5 hours in Fig.6. RhB self-degradation was very weak in the comparing experiment. The degradation rates of RhB were significantly different under composites $Mn_xZn_{1-x}Fe_2O_4$/β-Bi_2O_3 (10 wt %, 15 wt %, 20 wt %). It was expressed at detail that the degradation rate with $Mn_xZn_{1-x}Fe_2O_4$/β-Bi_2O_3 (15 wt%) reached 99.1% in the same condition, while excessive $Mn_xZn_{1-x}Fe_2O_4$ resulted in the degradation rate lower than that of pure β-Bi_2O_3. Namely, the photocatalytic activity of $Mn_xZn_{1-x}Fe_2O_4$/β-Bi_2O_3 (15 wt%) was the highest. Furthermore, the degradation rate in the irradiation period of 2-2.5 hour is much higher than before. We will explain this phenomenon as follows. Firstly, the photocatalyst and the RhB solution reach absorption equilibrium entirely after stirring and irradiation for 2 h. Photo-electrons and holes migrating to the surface of the composite catalyst also reach balance. Secondly, the phenomenon appeared (especially 10wt%, 15wt% and 20wt%). It is because a constant magnetic field causes electrons to do directional movement at a constant speed. The valence band of stimulated electronics (composites of 10wt%, 15wt% and 20wt%) did not accumulate in a place completely. So the phenomenon of the above three kinds of photocatalyst was more obvious.

It was more important that, M_r of $Mn_xZn_{1-x}Fe_2O_4$/β-Bi_2O_3 (15 wt%) was 7.01$A\cdot m^2\cdot kg^{-1}$, meaning the composite produced a stable magnetic field. As we all know, a constant magnetic field caused electrons to do directional movement at a constant speed. Some of the electrons did uniform motion along the magnetic field direction, but the other part did uniform circular motion perpendicular to the plane of the magnetic field[36-37]. Combined with the movement of electrons in a constant magnetic field, photo-generated electrons brought directional movement if a constant magnetic field was charged around the photocatalyst. Furthermore, a constant magnetic field promoted the bidirectional shunt (as Fig.7) of photo-generated electrons(e^-)[38]. So, valence band of electronics stimulated did not accumulate in a place. Based on these, the utilization efficiency of light energy (namely, the photoelectric conversion efficiency) increased. It was true that the photocatalytic activity was improved.

In addition, $Mn_xZn_{1-x}Fe_2O_4$ were able to absorb the most solar photons and increase the light response of β-Bi_2O_3 [39]. The action helped to absorb more incident photons and produced more photo-produced electrons(e^-) and holes(h^+), improving the photocatalytic activity. Magnetic field yielded by $Mn_xZn_{1-x}Fe_2O_4$ promoted the charged particles to move by specific roles, inhibiting the recombination of photo-generated electron-hole pairs and extending the lifetime of the photo-generated pairs. As a result, the photocatalytic activity was raised. We cannot ignore that $Mn_xZn_{1-x}Fe_2O_4$ is semiconductor, so it would become the recombination center of photo-produced electrons(e^-) and holes(h^+) and lowered the photocatalytic activity if load too much.

3.5 Recycling ability and stability

0.2g of $Mn_xZn_{1-x}Fe_2O_4$/β-Bi_2O_3 (15 wt%) was weighed and added into RhB solution of a concentration of 10mg/L (100mL), then carried out the photocatalytic experiments under simulated

sunlight. After the reaction of system completed, $Mn_xZn_{1-x}Fe_2O_4/\beta$-$Bi_2O_3$ and supernatant liquid were separated by an external magnetic field. The recovered composites were washed by anhydrous ethanol several times and then activated at a temperature of 60 □ for 2h. The dried solid was 0.1786g, so the recovery rate was 89.3%.

The stability and recyclability of $Mn_xZn_{1-x}Fe_2O_4/\beta$-$Bi_2O_3$ (15 wt%) was studied by recycling experiments. It was easy to get in Fig.8 that RhB degradation rate with the composite magnetic photocatalyst was 99.1% and 82.7% at 1st and 5th cycles. The experimental results revealed the composites could be reused several times without a significant decrease of the activity. After five recycles, the magnetic property parameter was illustrated in Fig.9 in contrast with the original magnetic data. M_s and M_r of the recycled composite in Fig.9 were respectively 5.37 and 0.39 $A \cdot m^2 \cdot kg^{-1}$ after five t recycles. Compared to the original magnetic data, saturation magnetization presented a litter lower. This was due to a loss in recovery process, resulting in decrease of magnetic substance for per unit mass. The coercivity and residual magnetization were not changed, indicating that the composites had the stable magnetic properties relatively. The above data showed that $Mn_xZn_{1-x}Fe_2O_4/\beta$-$Bi_2O_3$ (15 wt %) was indicative of high stability and good repeatable property.

M_s and M_r of the recycled composite in Fig.9 were respectively 5.37 and 0.39 $A \cdot m^2 \cdot kg^{-1}$ after five recycles use, and the coercivity and residual magnetization did not change. So, $Mn_xZn_{1-x}Fe_2O_4/\beta$-$Bi_2O_3$ (15 wt%) was indicative of high stability and good repeatable property.

4. Conclusions

The composite magnetic photocatalyst $Mn_xZn_{1-x}Fe_2O_4/\beta$-$Bi_2O_3$ (15 wt%) was synthesized by dip-calcination method. The synthesis was adapted to facilitate scale production for the simple preparation technology and low-cost procedure. Photocatalytic activity was evaluated with the degradation rate of RhB under simulated sunlight. VSM test results indicated that the composite possessed good magnetic properties, which was conducive to the separation and reuse. Recycling experiments showed that the recovery rate was up to 89.3%, and the degradation rate of RhB in the composite magnetic photocatalyst was from 99.1% down to 82.7% after five cycles. The composite was indicative of higher excellent catalytic activity and stability. The photocatalytic mechanism of the composite was discussed, and the magnetic photocatalyst produced a more stable magnetic field and increased the utilization efficiency of light, prompting the bidirectional shunt of photo-generated e^--h^- pairs. $Mn_xZn_{1-x}Fe_2O_4$ was able to absorb a great amount of solar photons, and increase the intensity of the light response of β-Bi_2O_3.

Acknowledgements

The authors are grateful for the support from the National Natural Science Foundation of China (NSFC.51374259) , the Fundamental and advanced research projects of Chongqing Science and Technology Commission (2013jjB20001), and Fundamental and Chongqing Graduate Student Research Innovation Project (CYB14040).

References

[1] A. H. K. Fujishima, Nature, 1972, 238, 37-39.
[2] J. H.Carey, J.Lawrence, H.M.Tosine, B. Environ. Contam. Tox., 1976, 16, 697-701.
[3] S. N. Frank, A. J. Bard, J. Am. Chem. Soc., 1977, 99, 303-308.
[4] S. N. Frank, A. J. Bard, J. Chem. Phys., 1977, 81, 1484-1489.
[5] S. N. Frank, A. J. Bard, J. Am. Chem. Soc., 1977, 14, 4667-4675.

[6] C. Ooka, S. Akita, Y. Ohashi, J. Mater. Chem., 1999, 9, 2943-2952
[7] A. N. Murashkevich, O. A. Alisienok, I. M. Zharskiy, E. K. Yukhno. J. Sol-Gel. Sci. Techn., 2013, 65, 367-373.
[8] L. G. Devi, R. Kavitha, RSC. Adv., 2014, 4, 28265-28299.
[9] M. S. Zhu, P. L. Chen, M. H. Liu, January, 2013, 58, 84-91.
[10] Y. H. Yan, H. Y. Guan, S. Liu, R. Y. Jiang, Ceram. Int., 2014, 40, 9095-9100
[11] W. Y. Shan, X. F. Bai, Chem. Adhesion., 2009, 31, 35-38
[12] X. J. Lu, P. Yin, Z. Z. Han. Front. Optoelectron., 2012, 5, 439-444
[13] X. L. Dong, Y. Shao, X. X. Zhang, H. C. Ma, X. F. Zhang, F. Shi, C. Ma, M. Xue, Res. Chem. Intermediat., 2014, 40, 2953-2961
[14] Y. Wang, Z. Q. Shi, C. M. Fan, X. G. Hao, G. Y. Ding, Y. F. Wang, Int. J. Min. Met. Mater., 2012, 19, 467-472.
[15] T. T. Lea, M. S. Akhtara, D. M. Parka, J. C. Leec, O. B. Yang. Appl. Catal. B-Environ., 2012, 111-112, 397-401
[16] Y. J. Li, T. P. Cao, C. L. Shao, C. H. Wang, Int. J. Inorg. Mater., 2012, 27, 687-692.
[17] M. Drache, P. Roussel, J. P. Wignacourt, Chem. Rev., 2007, 107, 80-96.
[18] A. Cabot, A. Marsal, J. Arbiol, et al, Sensor. Actuat. B-Chem., 2004, 99, 74-89.
[19] L. J. Xu, L. Y. Huang, C. L. Liu, T. P. Xie, Chinese Patent, CN103447054A.
[20] A. A. Aziz, Y. H. Yau, G. L. Puma, C. Fischer, S. Pichiah, Chem. Eng. J., 2014, 235, 264-274.
[21] K. S. Chee, M. Daimu, A. Nobuyasu, O. Toshitaka. J. Am. Ceram. Soc., 2009, 45, 34-39.
[22] G. Thirupathi, R. Singh, AIP Conf. Proc., 2013, 1591, 470-471.
[23] S. H. Wang, S. Q. Zhou, Appl. Surf. Sci., 2010, 256, 6191-6198.
[24] C. Xie, L. J. Xu, Y. J. Ye, X. Y. Li, S. Y. Wang, Chin. J. Geochem., 2015, 34, 219-223.
[25] H. F. Cheng, B. B. Huang, J. B. Lu, Z. Y. Wang, B. Xu, X. Y. Qin, X. Y. Zhang, Y. Dai, Phys. Chem. Chem. Phys., 2010, 12, 15468-15475.
[26] Q.H.Yan, L.Yang, L.J.Yang, Chin. J. Pharm. Anal.,2011,31,1393-1396(chinese)
[27] H.F.Shi,Spectroscopy and spectral analysis, 2004,24,229-232(chinese)
[28] X.M.Tang, X.R.Ren, Y.Q.Fang, Res. Environ.Eng.,2013,27,831-834(chinese)
[29] T. P. Xie, C. L. Liu, L. J. Xu, J. Yang, W. Zhou, J. Phys. Chem. C, 2013, 117, 24601-24610.
[30] N. Pugazhenthiran, P. Sathishkumar, S. Murugesan, S. Anandan, Chem. Hem. Eng. J., 2011, 168, 1227-1233.
[31] Y. F. Qiu, M. L. Yang, H. B. Fan, Y. Z. Zuo, Y. Y. Shao, Mater. Lett., 2011, 65, 780-782.
[32] O. Monnereau, L. Tortet, P. Llewellyn, F. Rouquerol, G.Vacquier, Solid State Ionics, 2003, 157, 163-169.
[33] T. Sakata, J. Photoch. Photobio., 1985, 29, 205-215.
[34] Y. Yang, H. Zhong, C. X. Tian, Res. Chem. Intermediat., 2011, 37, 91-102.
[35] T. Sakata, J. Photochem., 1985, 29, 205-215.
[36] H. Kisch, Angew. Chem. Int. Ed., 2013, 52, 812-847.
[37] C. F. Li, Q. Wang, Physica B, 1999, 269, 22-27.
[38] M. Torres, A. Kunold, Phys. Lett. A, 2004, 323, 290-297.
[39] B. Neppolian, Y. Kim, M. Ashokkumar, H. Yamashita, H. Choi, J. Hazard. Mater., 2010, 182, 557-562.

Appendices

Figure captions

Fig.1 XRD spectra of pure β-Bi_2O_3 and $Mn_xZn_{1-x}Fe_2O_4$ as well as composite $Mn_xZn_{1-x}Fe_2O_4$/β-Bi_2O_3 (15 wt %)

Fig.2 The FTIR spectra of pure β-Bi_2O_3 and composite $Mn_xZn_{1-x}Fe_2O_4$/β-Bi_2O_3(15 wt %)

Fig.3 SEM images of pure β-Bi_2O_3 and composite $Mn_xZn_{1-x}Fe_2O_4$/β-Bi_2O_3 (15 wt %) (10μm、2μm)

Fig.4 Diffuse reflectance spectra and corresponding band gap of pure β-Bi_2O_3 and composite magnetic photocatalyst $Mn_xZn_{1-x}Fe_2O_4$/β-Bi_2O_3(15 wt %)

Fig.5 The magnetic hysteresis loop of $Mn_xZn_{1-x}Fe_2O_4$ and the composite $Mn_xZn_{1-x}Fe_2O_4$/β-Bi_2O_3(15 wt%)

Fig.6 Photocatalytic properties of pure β-Bi_2O_3 and $Mn_xZn_{1-x}Fe_2O_4$/β-Bi_2O_3 (5 wt %, 10 wt %, 15 wt %, 20 wt %, 25 wt %)

Fig.7 The photocatalytic mechanism of $Mn_xZn_{1-x}Fe_2O_4$/β-Bi_2O_3 (15 wt%)

Fig.8 The recycle experiments of degrading RhB on the composite $Mn_xZn_{1-x}Fe_2O_4$/β-Bi_2O_3 (15 wt%) under simulated sunlight irradiation

Fig.9 The magnetic hysteresis loop of $Mn_xZn_{1-x}Fe_2O_4$/β-Bi_2O_3 (15 wt %) and composites after five recycles

Table captions

Table 1 The effect of mass ratio, reaction time and calcination temperature on the degradation rate of RhB

Table 2 The experimental levels and factors of the orthogonal experimental design

Table 3 ICP analysis of $Mn_xZn_{1-x}Fe_2O_4$/β-Bi_2O_3 (15 wt%)

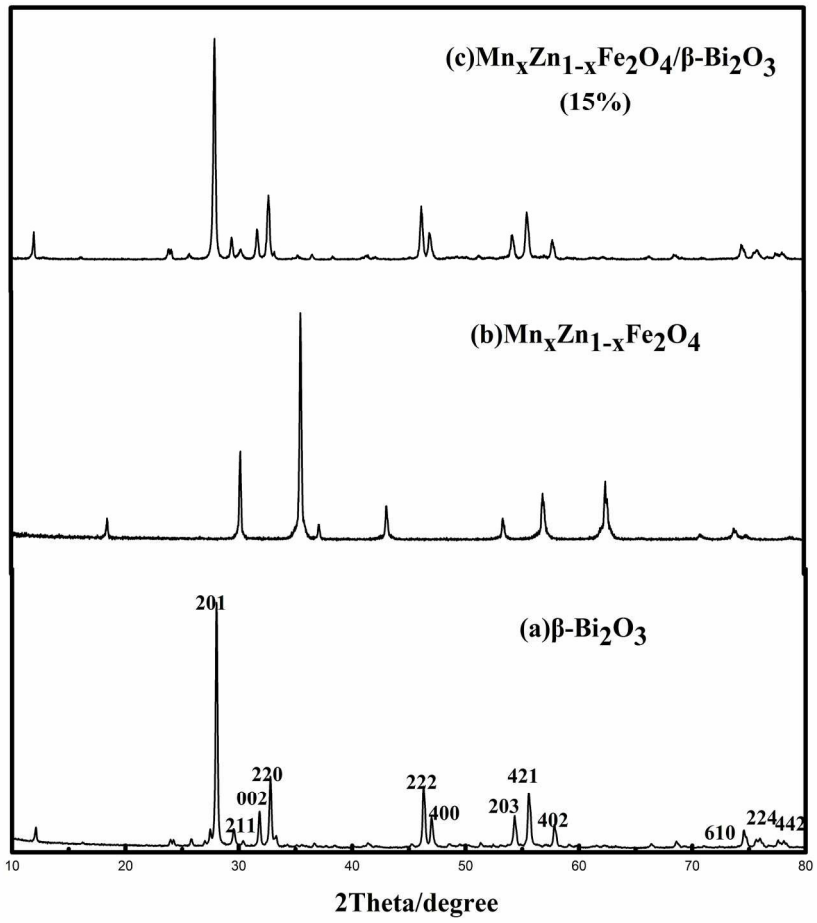

186x202mm (300 x 300 DPI)

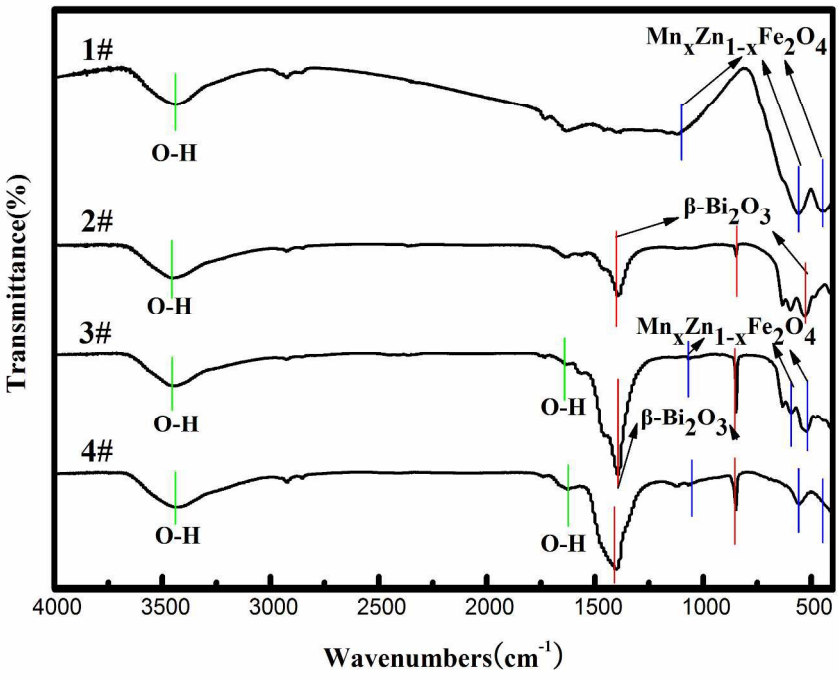

260x218mm (300 x 300 DPI)

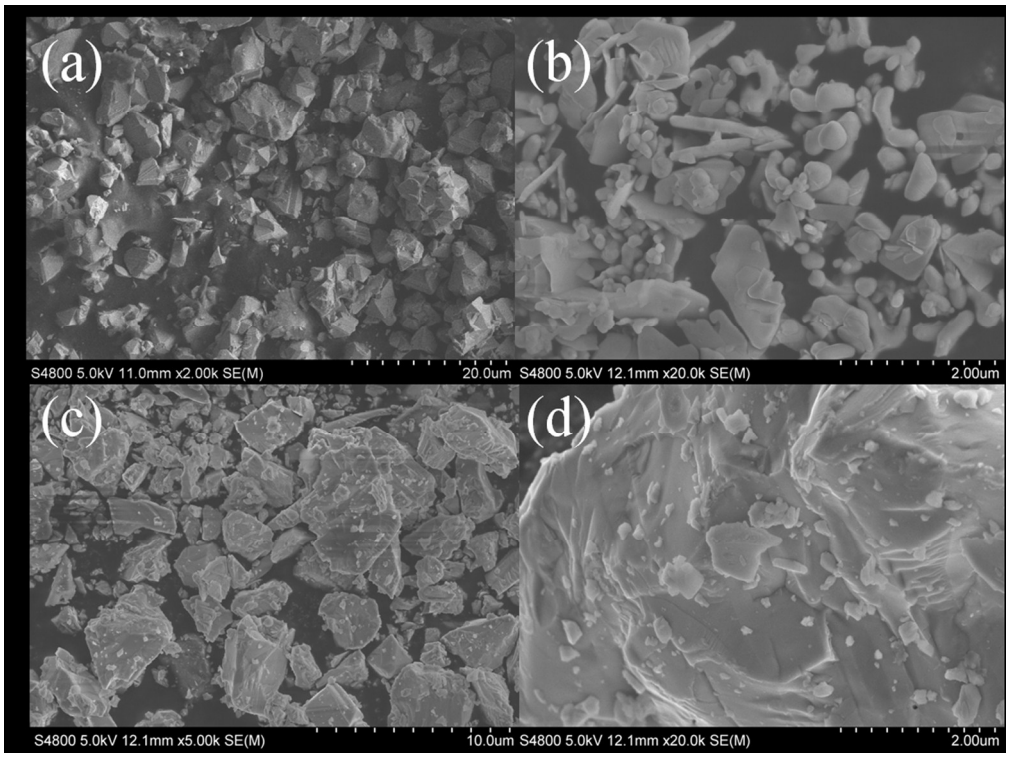

196x146mm (150 x 150 DPI)

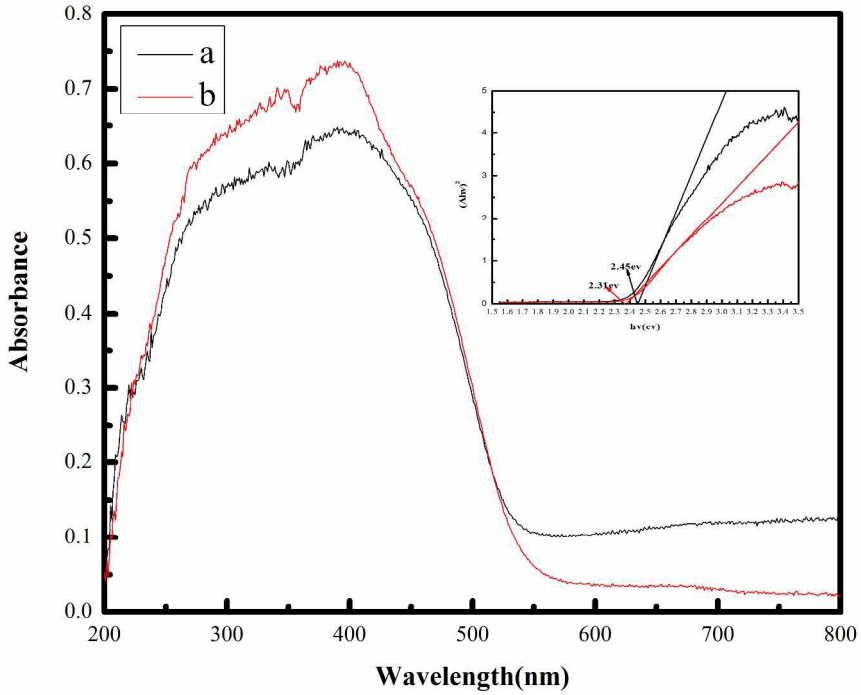

259x218mm (300 x 300 DPI)

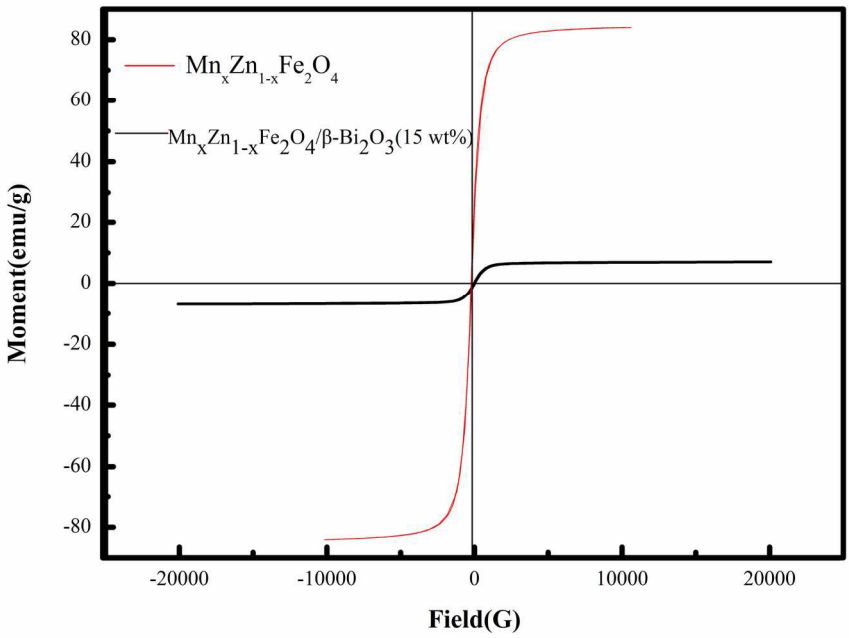

173x136mm (300 x 300 DPI)

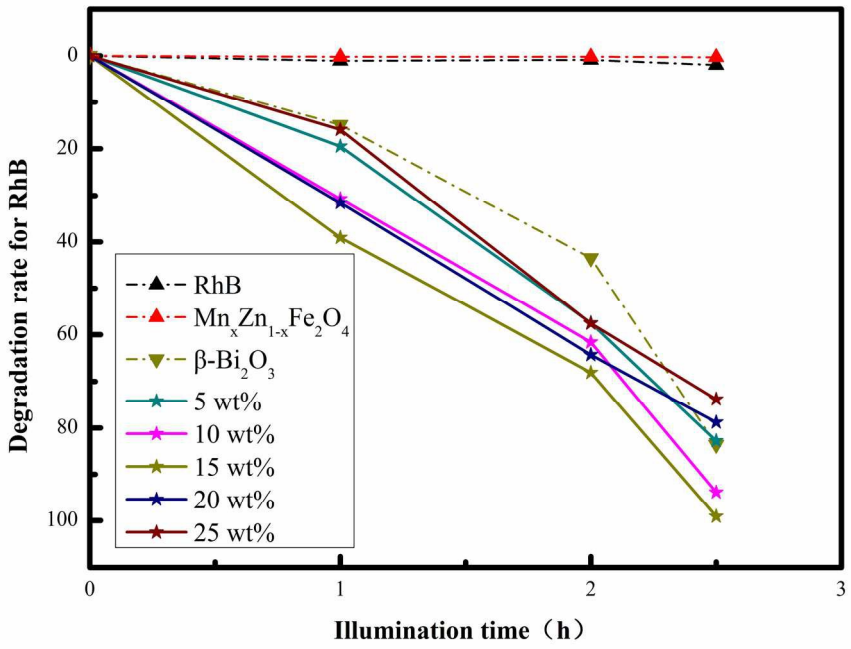

173x139mm (300 x 300 DPI)

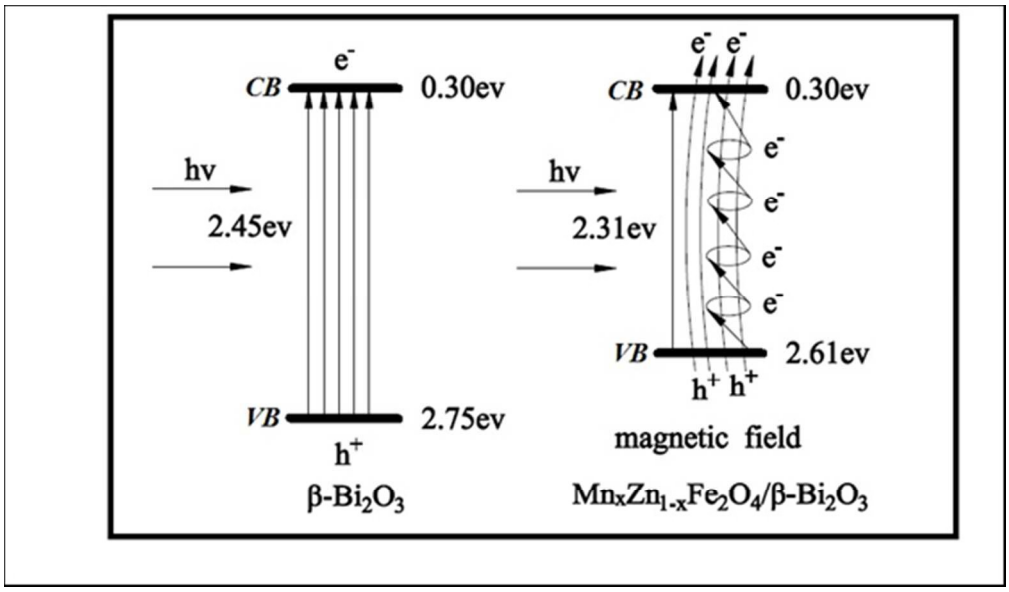

104x60mm (150 x 150 DPI)

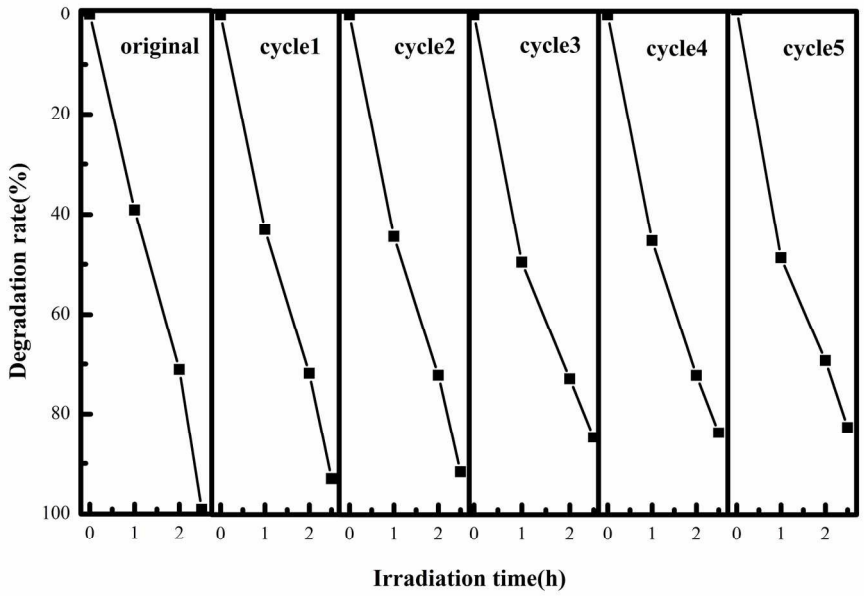

175x128mm (300 x 300 DPI)

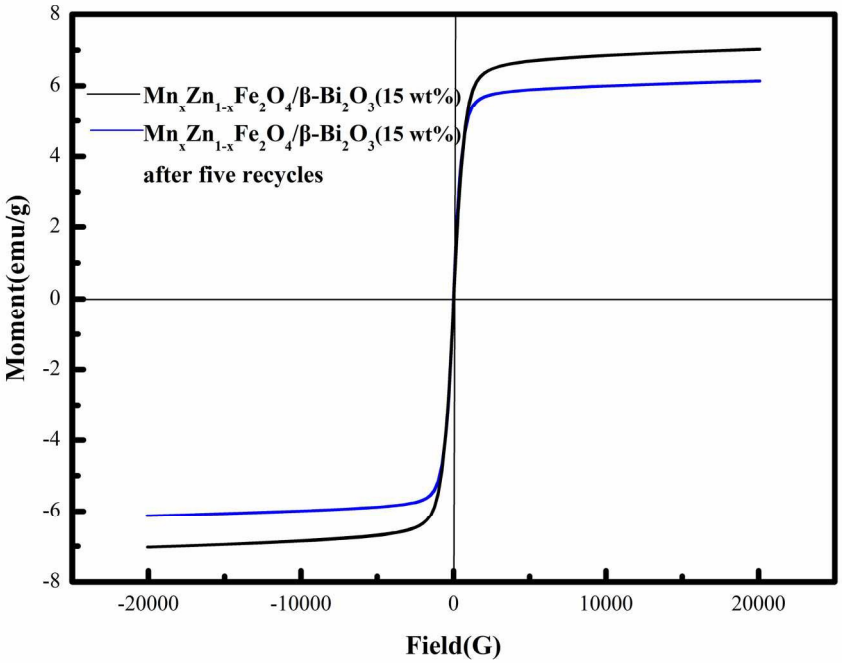

173x141mm (300 x 300 DPI)

Table 1 The influence of mass ratio and reaction time as well as calcination temperature on the degradation rate of RhB

mass ratio （wt%）	degradation rate（%）	reaction time （h）	degradation rate（%）	calcination temperature （□）	degradation rate（%）
5	82.8	1	80.8	360	63.6
10	93.9	1.5	86.4	370	90.6
15	99.1	2	98.7	380	99.5
20	78.7	2.5	77.7	390	76.6
25	73.8	3	70.2	400	72.5

Table 2. The orthogonal experimental design

	Factor 1	Factor 2	Factor 3
	Mass ratio, wt%	Reaction time, h	Calcination temperature, □
Level 1	10	1	370
Level 2	15	2	380
Level 3	20	3	390

Table 3 ICP analysis of $Mn_xZn_{1-x}Fe_2O_4/\beta$-$Bi_2O_3$ (15 wt%)

Elements	Bi			Mn			Zn			Fe		
Wavelength/nm	190.2	195.4	223.0	257.6	293.9	348.2	213.8	328.2	481	234.3	259.9	322.7
Signal intensity	117100	14810	242200	804000	188600	22300	103300	1197	16600	177200	364500	3438
	117100	14830	239700	793500	187600	22230	101900	1183	16500	178500	365200	3455
	117200	14810	239900	787000	182700	21720	101900	1181	16110	178700	351700	3404
Average signal intensity	117133	14817	240600	794833	186300	22083	102367	1187	16403	178133	360467	3432
Ratio	8:1:16			36:8:1			86:1:14			52:105:1		